Modeling of the shared magnets of the ATF Extraction Line

M. Alabau Pons, A. Faus-Golfe, P. Bambade, G. Le Meur, F. Touze

Modeling of the shared magnets of the ATF Extraction Line

M. Alabau Pons, A. Faus-Golfe[1], P. Bambade, G. le Meur, F. Touze[2]

1) IFIC (CSIC-UV), Valencia, Spain
2) LAL, Univ. Paris-Sud, CNRS/IN2P3, Orsay, France

Abstract

After extraction from the ATF Damping Ring, the linear beam optics is matched before injection into a section dedicated to beam diagnostics. Experimentally, vertical emittances in this section have since several years been observed to be larger than expected, by factors of two to three, with a seemingly strong dependence on intensity. This has motivated studies of the possible sources of emittance growth. One of these is thought to be the non-linearity experienced by the beam during the extraction, as it is transported off-axis through several magnets which are shared with the Damping Ring. Such non-linearity can generate a sensitivity of the emittance to the orbit parameters in the extraction, which would be very undesirable in the newly built ATF2 final focus system, where the same extraction line is used. In this report, a detailed calculation of the modeling of these shared magnets is presented, in order to quantify the magnitudes of both the linear and non-linear fields to be used in the evaluation of the optics and in tracking simulations of the performance of the extraction line.

Contents

1 Introduction

The Accelerator Test Facility (ATF) at KEK (Japan) is a Damping Ring (DR) built to demonstrate the small emittance beams needed for future linear colliders [1]. It has achieved world records for the normalized vertical emittance, with values as small as 3 x 10^{-8} m rad at 1.3 GeV. ATF2 is a prototype final focus system, recently completed as a result of an international collaboration to study the feasibility of focusing the damped ATF beam down to nanometer-scale spot sizes. Such small spots are required at the Interaction Point (IP) of the future linear colliders, and ATF2 uses the same principle of local chromaticity correction [2] as in the ILC and CLIC projects. One of the main goals of ATF2 is the establishment of the hardware and beam handling technologies pertaining to achieving and measuring such small beams, reproducibly and in stabilised conditions. The nominal vertical beam size is specified to be 37 nm at the ATF2 final focus point. For this, beams with the smallest vertical emittances must both be provided by the ATF Damping Ring (DR) and preserved throughout the different sections of the optical transport.

The layout of the Extraction Line (EXT) used to drive the beam from ATF to ATF2 is shown in Fig. 1. After extraction, there is a section for beam diagnostics. In this section, measured vertical emittances have often been found larger than expected, with moreover a strong dependence with beam intensity, as shown in Fig. 2 [3]. This has motivated the study of several possible sources of emittance growth, among which non-linear fields that the beam experiences when passing off-axis through some of the magnets in the extraction line which are shared with the DR.

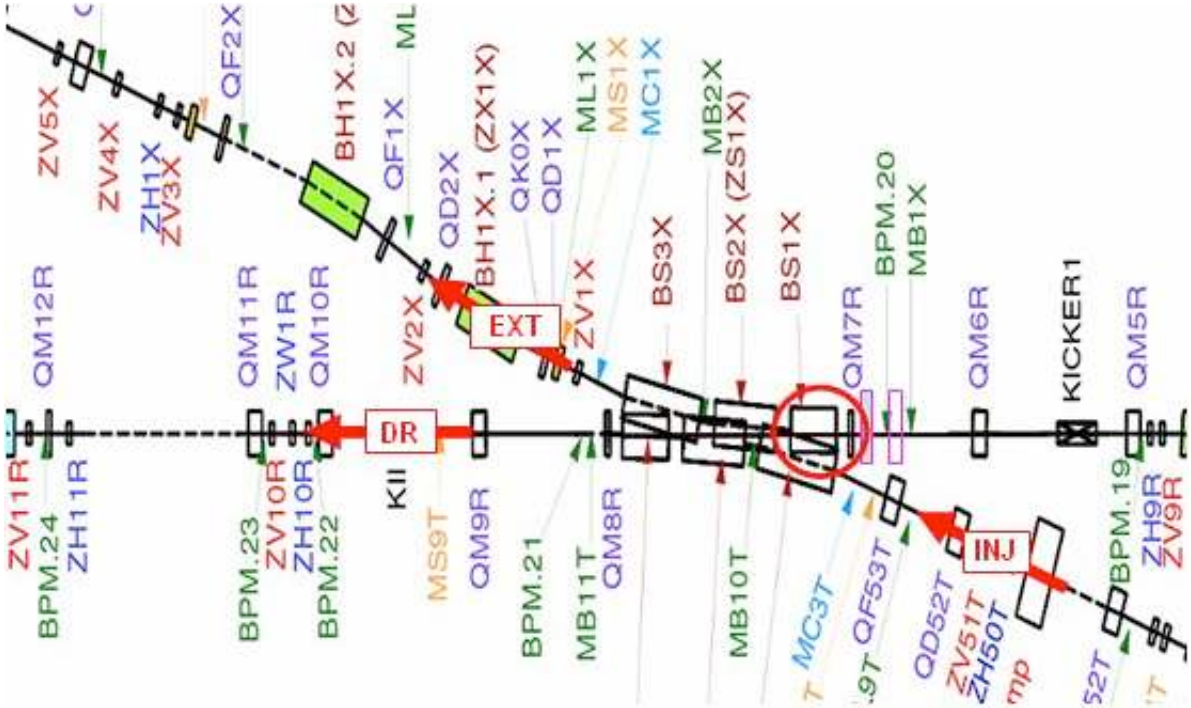

Figure 1: Layout of region around the beam extraction.

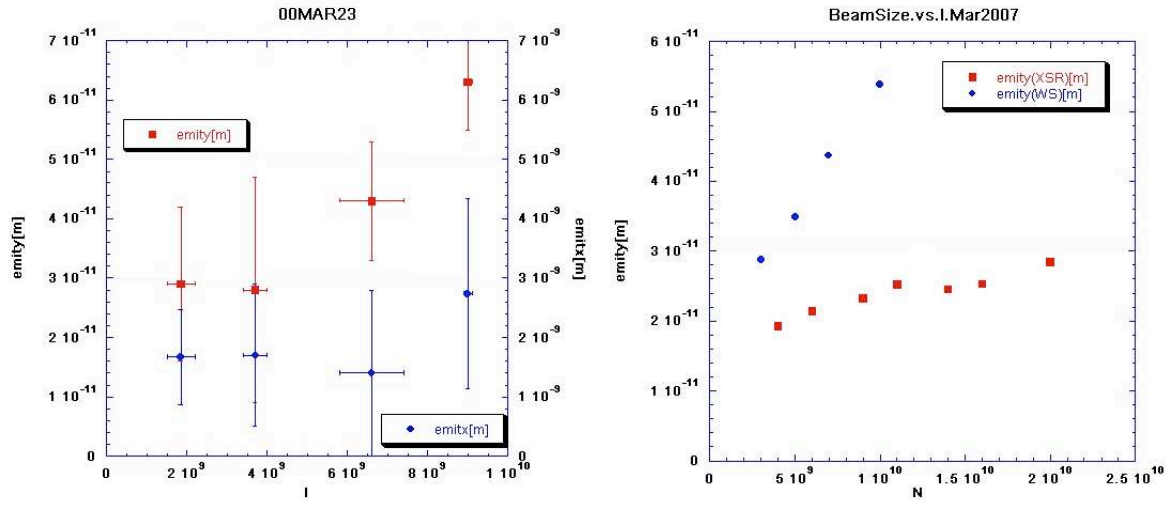

Figure 2: (a) Vertical Emittance versus Intensity in 2000; (b) Vertical Emittance versus Intensity in 2007.

In this report, a detailed evaluation of the field maps of the shared magnets in the extraction line is presented, using the code PRIAM [4]. The computed field maps are fitted as two-dimensional multipole expansions to obtain continuous representations suitable for tracking simulations. The results are compared with previous work based on the code POISSON [5]. Finally some conclusions are outlined.
This study is important to assess the contribution of the non-linearity in the extraction line to the increased emittance. It is of special relevance to ATF2 since the extraction line was not redesigned and since most of its shared magnets will remain unchanged.

2 The ATF extraction line

The ATF EXT line is divided in three regions: 1) EX0: shared with the DR, 2) EX1: matching area and 3) EX2: dispersion free diagnostic area. The optics description of this line, calculated with the MAD program [6], are shown in Fig. 3.
The region EX0 containing the shared magnets studied in this report is composed mainly of a kicker (KE1X), a vertical focusing quadrupole (QM6R), a horizontal focusing quadrupole (QM7R), and three septums (BS1X, BS2X, BS3X) (see Fig. 1). Extraction is initiated by firing the kicker. This causes the beam to pass off-axis through the magnetic elements of the EX0 region. For example, as can be seen in Fig. 4, the extracted beam path is significantly beyond the expected linear region of the QM7R quadrupole. Tab. 1 summarizes the off-axis positions in the elements of the EX0 region. For quadrupoles, distances are referred to the center of the magnet, while for septum magnets they are referred to the edge of the innermost conductor. After passage through the three septums, the extracted beam is transported in an independent magnetic channel.

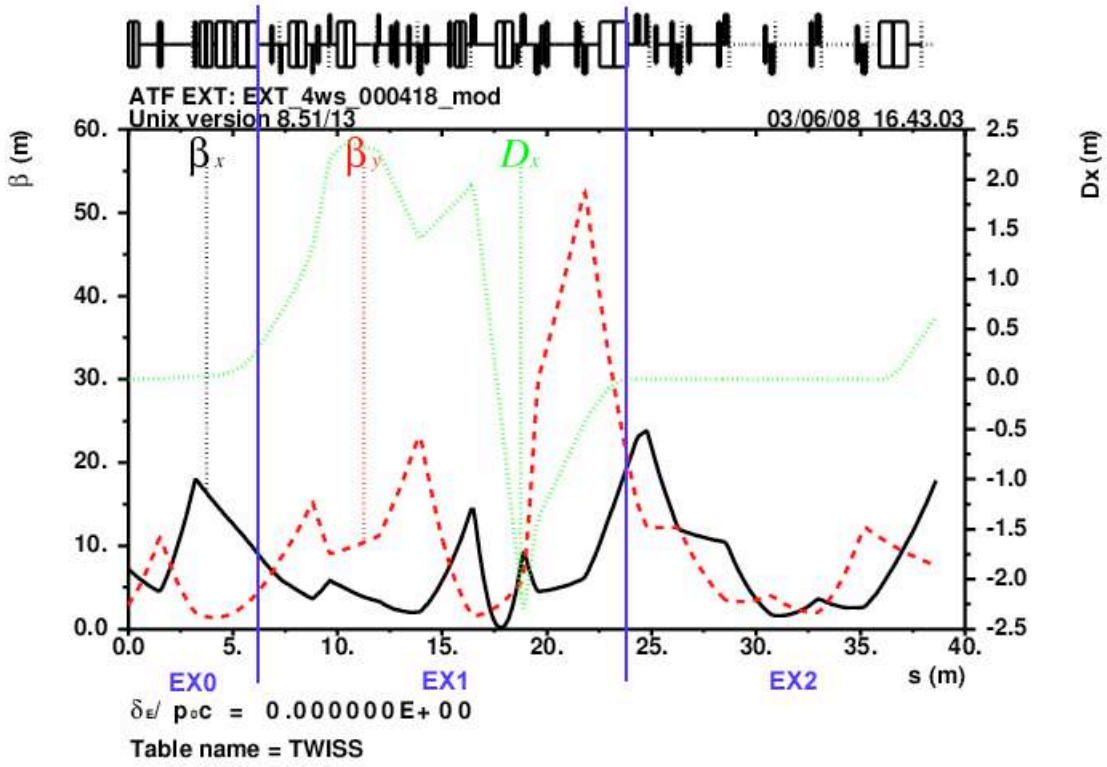

Figure 3: Optics calculation of the ATF EXT line.

The off-axis transport through the EX0 magnets is represented in the description of the optics by means of dipole components complemented by sets of normal multipoles, both permitted and non-permitted for a quadrupole. The latter are a potential source of vertical emittance growth in the ATF EXT line. They are computed in the following section as input to the tracking programs used to estimate the vertical emittance growth.

Type	**Element name**	x [mm]	y [mm]	
Quadrupole	QM6R	6.5	0.0	distance from
Quadrupole	QM7R	22.5	0.0	center of quad.
Septum	BS1X	8.2	0.0	distance from
Septum	BS2X	15.3	0.0	end of the top half
Septum	BS3X	16.0	0.0	septum conductor

Table 1: Off-axis displacement for some of the EX0 elements.

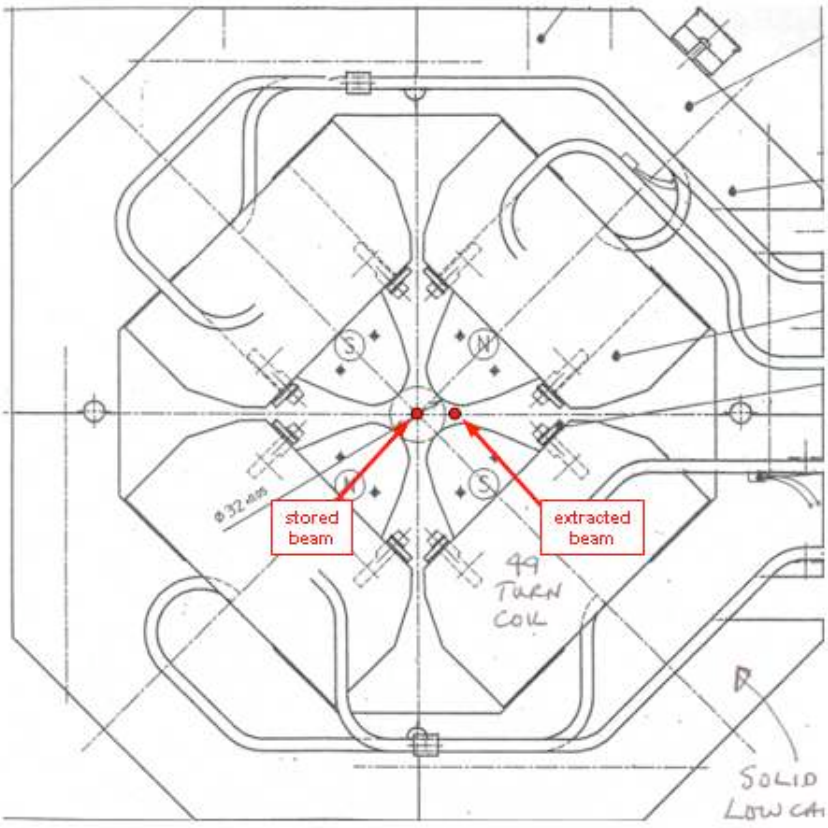

Figure 4: QM7R draft with stored and extracted beam position.

3 Field mapping for quadrupole QM7R using PRIAM

The field mapping for the QM7R quadrupole magnet was made in two steps: computation of the magnetic field on a finite element mesh, and fitting by polynoms in order to get a continuous representation in the complex plane.
The finite element code PRIAM [4] was used for the magnetic field calculations. A brief description of PRIAM is provided in Appendix 1. The polynomial fits were done with MINUIT [7].
Below, before computing and fitting the field map for QM7R, a description of the formalism used to obtain a continuous representation of the field in a magnet is presented.

3.1 Local representation of the magnetostatic field in two dimensions

3.1.1 The potentials and magnetic field as analytical functions

The magnetic field $\vec{B}$ derives from a vector potential $\vec{A}$ through the relation : $\vec{B} = rot(\vec{A})$. When the magnetic field has only two components B_x and B_y, the last relation reduces to:

$$B_x = \frac{\partial A_z}{\partial y} \; ; \; B_y = -\frac{\partial A_z}{\partial x}$$

Setting the flux function $\Phi = A_z$ one gets:

$$B_x = \frac{\partial \Phi}{\partial y} \; ; \; B_y = -\frac{\partial \Phi}{\partial x}$$

The curves $\Phi = cst$ are the field lines and their orthogonal trajectories, $V^* = cst$ are scalar potential lines from which derives the magnetic field: $\vec{B} = -grad(V^*)$. For a complex potential in the form of an analytic function:

$$\zeta(z) = \Phi(x, y) + iV^*(x, y)$$

where $z = x + i.y$ is the complex variable, the conditions for analyticity are:

$$\frac{\partial \Phi}{\partial x} = \frac{\partial V^*}{\partial y} \; ; \; \frac{\partial V^*}{\partial x} = -\frac{\partial \Phi}{\partial y}$$

which entails:

$$-\frac{d\zeta}{dz} = -\frac{\partial \Phi}{\partial x} + i.\frac{\partial \Phi}{\partial y} = -\frac{\partial V^*}{\partial y} - i.\frac{\partial V^*}{\partial x} = B_y + iB_x = B(z)$$

If ζ is analytical, so is B(z). The analyticity conditions for B then reads:

$$\frac{\partial B_y}{\partial x} = \frac{\partial B_x}{\partial y} \; ; \; \frac{\partial B_x}{\partial x} = -\frac{\partial B_y}{\partial y}$$

which are *Maxwell equations* in two dimensions (in the absence of currents):

$$rot(\vec{B}) = 0 \; ; \; div(\vec{B}) = 0$$

3.1.2 The multipoles

Let's consider as potential $\zeta(z) = -B_0 z$. The derivation leads to:

$$B(z) = B_y = B_0$$

which is a pure *dipole* field. The field lines are $\Phi(x, y) = -B_0 x = cst$, whereas the potential lines are $V^*(x, y) = y = cst$.
With the potential $\zeta(z) = -\frac{1}{2}G.z^2 = -\frac{1}{2}G(x^2 - y^2 + 2ixy)$, the magnetic field reads :

$$B(z) = Gx + iGy$$

i.e. $B_x = Gy$ and $B_y = Gx$ which is a pure *quadrupole* field. The field lines are $\Phi(x, y) = -\frac{1}{2}G(x^2 - y^2) = cst$, i.e. hyperboles as well as the potentials lines $V^*(x, y) = -\frac{1}{2}Gxy = cst$. To obtain a pure *sextupole* field one has to take the potential proportional to $\zeta(z) = -z^3$.

3.1.3 Polynomial fits

Usually the field in the magnets of a beam transport system is known at discrete points in a limited region, either from measurements or from computer simulations. For computer tracking purposes, it is generally necessary to know the magnetic field in continuous form in order to avoid instabilities in the computations. A solution is to represent the magnetic field by analytic expressions obtained by fits to the known values. A convenient way is to use an integer series of the complex variable, with complex coefficients, around a reference point:

$$B(z) = B_y + iB_x \sim \sum_{n=0}^{N} a_n z^n$$

The real part of the complex coefficients a_n is known as *normal multipoles* and the imaginary part as *skew multipoles*. Such a representation is consistent with the nature of the magnetic field. In particular the property of analyticity entails that Maxwell equations are satisfied. This is generally not the case for other polynomial fits. Obviously, to benefit from this physical constraint, the fitting must be done in two dimensions.
In the particular case of symmetry with respect to the axis (plane) $y = 0$, i.e. $B_x(x, -y) = -B_x(x, y)$ and $B_y(x, -y) = B_y(x, y)$, the coefficients a_n become real. Indeed, for every z, this condition can be written: $B(\overline{z}) = \overline{B}(z)$
or :

$$\sum_{n=0}^{N} a_n \overline{z}^n = \sum_{n=0}^{N} \overline{a_n}.\overline{z}^n$$

where $\overline{z}$ denotes the conjugate of z and which implies: $\overline{a_n} = a_n$.
Separate expansions of B_x and B_y can be obtained as polynoms of the variables x and y. Namely, recalling that: $(x+iy)^k = \sum_{p=0}^{k} C_k^p (iy)^{k-p} x^p$, with $C_m^p = \frac{m!}{p!(m-p)!}$ and the convention $C_m^0 = 1$, one obtains:

$$B_x = y \sum_p \sum_{q=0}^{p} (-1)^{p+q} x^{2q} \left(a_{2p+1} C_{2p+1}^{2q} + a_{2p+2} C_{2p+2}^{2q+1} x \right) y^{2(p-q)}$$

and:

$$B_y = \sum_p \sum_{q=0}^{p} (-1)^{p+q} x^{2q} \left(a_{2p} C_{2p}^{2q} + a_{2p+1} C_{2p+1}^{2q+1} x \right) y^{2(p-q)}$$

It can be noticed that B_x is the product of y by a polynom $H(x, y)$. For fixed x, H can be reordered with respect to the sole variable y, with only even powers y^{2h} appearing with coefficients:

$$\alpha_{2h} = \sum_{q=0} (-1)^h x^{2q} \left(a_{2h+2q+1} C_{2h+2q+1}^{2q} + a_{2h+2q+2} C_{2h+2q+2}^{2q+1} x \right)$$

3.1.4 For MAD users

The multipole expansions for normal and skew field components defined in MAD are:

$$B_y(x,0) = \sum_k \frac{B_{kn} x^k}{k!} \; ; \; B_x(x,0) = \sum_k \frac{B_{ks} x^k}{k!}$$

With the adopted symmetry with respect to the axis (plane) $y = 0$, all the skew multipoles vanish and the successive normal multipoles are:

- dipole : $B_{0n} = a_0$
- quadrupole : $B_{1n} = a_1$
- sextupole : $B_{2n} = 2 * a_2$
- .....
- 2k-pole : $B_{kn} = k! a_k$

The MAD coefficients $K_{kn} = B_{kn}/B_0\rho$ allow one to get the strengths of the multipoles $K_{kn}L$, in m^{-k}, multiplying $k!a_k$ by the length L of the element and dividing by the appropriate $B_0\rho$, where $B_0\rho$ [T m] = 10/2.998 E [GeV] is the magnetic rigidity.

3.2 Numerical results

3.2.1 QM7R

QM7R is a horizontally focusing quadrupole magnet, with an aperture of radius $r = 0.015995$ m and a length $L = 0.078907$ m. The focusing gradient is 21.8767 T/m. Fig. 5 shows the field lines in the computed structure (1/8th of the quadrupole, taking into account the symmetries). The fit around the center of the quadrupole ($x = 0.0$ m, $y = 0.0$ m) using the polynomial fit method described above provides the normal multipole coefficients listed in Tab.2. The value of the

$$\chi^2 = \sum_{allsampled\ points} \left[\|B_x^{fit} - B_x^{priam}\|^2 + \|B_y^{fit} - B_y^{priam}\|^2 \right]$$

for this fit is 0.014 T^2 (using 40400 sampled points). The multipole coefficient to be used in the MAD program [6], $K_{kn}L = B_{kn}L/B_0\rho$, are added for completeness, where the length of the magnet (L) has the value of 0.078907 m and the magnetic rigidity $B_0\rho$ [T m] = 10/2.998 E [GeV] is calculated for 1.3 GeV. Notice that only some orders (1,5,9, 13,...) are permitted in accordance with the quadrupole symmetry.
The zone of interest for the tracking of the extracted beam is near $x = 0.0225$ m, $y = 0.0$ m. The fit performed in a region around this point, defined by $0.0175 \leq x \leq 0.0275$ m and $0.0 \leq y \leq 0.004$ m, provides the coefficients summarized in Tab. 3. The value of the χ^2 (defined as above) for this fit is 0.0395 T^2 (for 5000 sampled points).

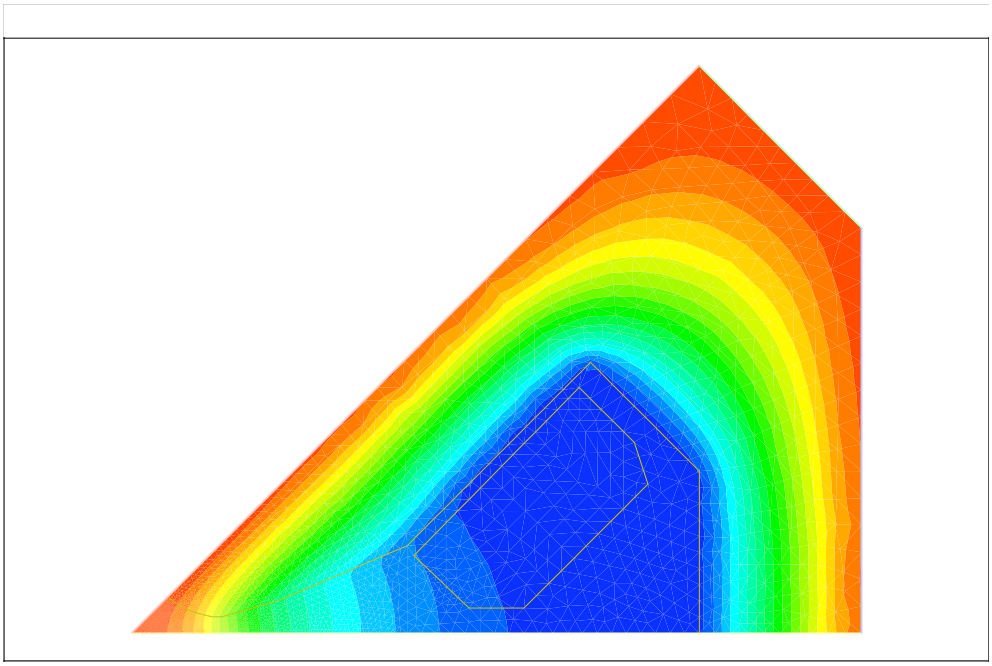

Figure 5: QM7R B field lines

Field Coefficient		units	**MAD Coefficient**		units
a_1	2.1780989 10^{1}	[T m^{-1}]	K_1L	3.9633533 10^{-1}	[m^{-1}]
a_5	1.1406000 10^{6}	[T m^{-5}]	K_5L	2.4905761 10^{6}	[m^{-5}]
a_9	-6.3613000 10^{-15}	[T m]$^{-9}$]	K_9L	-4.200334 10^{-11}	[m^{-9}]
a_{13}	0.0	[T m^{-13}]]	$K_{13}L$	0.0	[m^{-13}]

Table 2: Multipole coefficients for QM7R at the center of the quadrupole from the PRIAM mapping and fitted with a polynomial function using MINUIT.

It can be noticed that due to the displacement in the horizontal plane all the normal multipole components are permitted for QM7R. The main components are a dipole field (a_0), a quadrupole field (a_1) which is 23% less than on-axis, a sextupole field (a_2) and an octupole field (a_3). The other high order multipoles have decreasing values while the series is limited to 8^{th} order.
Fig. 6 compares the field values from PRIAM with the ones reconstructed from the fit for $y = 1, 2$ mm. Figs. 7 and 8 shows this comparison in two dimensions over the defined range.
In the MAD optics description of the EXT line, QM7R is simulated as a sector bend of length (L) 0.078907 m and angle -0.8942055 10^{-2} rad (the difference in the sign is a special convention in the MAD program), with a quadrupole component of strength 0.3980779044020 m^{-1}. Comparing with the value in Tab. 3, the dipole component has a slight difference of 2% while for the quadrupole component the difference is as large as 24%. The latter has a significant impact on the linear optics, as shown in Fig. 9 where it is compared to the design functions of

Field Coefficient		units	**MAD Coefficient**		units
a_0	4.8119811 10^{-1}	[T]	K_0L	8.7560676 10^{-3}	
a_1	1.6721776 10^{1}	[T m^{-1}]	K_1L	3.0427593 10^{-1}	[m^{-1}]
a_2	-1.2801437 10^{3}	[T m^{-2}]	K_2L	-4.6587984 10^{1}	[m^{-2}]
a_3	-1.5580988 10^{5}	[T m^{-3}]	K_3L	-1.7011062 10^{4}	[m^{-3}]
a_4	-5.1401980 10^{6}	[T m^{-4}]	K_4L	-2.2447929 10^{6}	[m^{-4}]
a_5	-6.2084000 10^{5}	[T m^{-5}]	K_5L	-1.3556000 10^{6}	[m^{-5}]
a_6	1.4791000 10^{4}	[T m^{-6}]	K_6L	1.9377000 10^{5}	[m^{-6}]
a_7	5.5069000 10^{2}	[T m^{-7}]	K_7L	5.0501000 10^{4}	[m^{-7}]
a_8	3.7827000 10^{1}	[T m^{-8}]	K_8L	2.7752000 10^{4}	[m^{-8}]
a_9	0.0	[T m^{-9}]	K_9L	0.0	[m^{-9}]
a_{10}	0.0	[T m^{-10}]	$K_{10}L$	0.0	[m^{-10}]
a_{11}	0.0	[T m^{-11}]	$K_{11}L$	0.0	[m^{-11}]
a_{12}	0.0	[T m^{-12}]	$K_{12}L$	0.0	[m^{-12}]

Table 3: Multipole coefficients for QM7R at $x = 0.0225$ m and $y = 0.0$ m from the center of the quadrupole from the PRIAM mapping fitted with a polynomial function using MINUIT.

Fig. 3. While effects on the horizontal dispersion (D_x) remain small, with a maximum deviation of $\pm 2.5\%$, large deviations of up to $\pm 20\%$ in the vertical beta function (β_y) and between -400% / +66% in the horizontal beta function (β_x) result from the weaker strength of QM7R seen by the extracted beam.

4 Field mapping for quadrupole QM6R

QM6R is a vertically focusing quadrupole of the EXT line which is also shared with the DR. It has an aperture of radius $r = 0.016$ m, a length $L = 0.198745$ m and a focusing gradient of -15.5377 T/m. As this magnet comes just after the kicker, the horizontal offset of the extracted beam is only 0.0065 m. As this is significantly less than the radius of the aperture, the non-linearity seen by the extracted beam is nearly negligible.

Fig. 10 shows the field lines in the computed structure (1/8th of the quadrupole, taking into account the symmetries). The fit around the center of the quadrupole ($x = 0.0$ m, $y = 0.0$ m) using the polynomial fit method described in the previous section provides the normal multipole coefficients listed in Tab.4. The value of the χ^2 for this fit is 9.720794 10^{-4} T^2 (for 40000 sampled points).

The zone of interest for the tracking of the extracted beam is near $x = 0.0065$ m, $y = 0.0$ m. The fit in a region around this point, defined by $0.005 \leq x \leq 0.008$ m and $0.0 \leq y \leq 0.0015$ m, provides the coefficients listed in Tab. 5. The value of the χ^2 for this fit is 4.391552 10^{-5} T^2 (for 5000 sampled points).

In the MAD optics description of the EXT line, QM6R is simulated as a sector bend of length (L) 0.198745 m and angle 0.462503985558 10^{-2} rad (the difference in the sign is a special con-

Field Coefficient		units	**MAD Coefficient**		units
a_1	-1.5531000 10^1	[T]	K_1L	-7.1181198 10^{-1}	[m^{-1}]
a_5	1.7035000 10^5	[T m^{-1}]	K_5L	9.3689141 10^5	[m^{-5}]
a_9	-1.2743000 10^4	[T m^{-9}]	K_9L	-2.1193398 10^8	[m^{-9}]
a_{13}	0.0	[T m^{-13}]	$K_{13}L$	0.0	[m^{-13}]

Table 4: Multipole coefficients for QM6R at the center of the quadrupole from the PRIAM mapping and fitted with a polynomial function using MINUIT.

Field Coefficient		units	**MAD Coefficient**		units
a_0	-1.0094000 10^{-1}	[T]	K_0L	-4.6262508 10^{-3}	
a_1	-1.5526000 10^1	[T m^{-1}]	K_1L	-7.1158282 10^{-1}	[m^{-1}]
a_2	-1.3721000 10^0	[T m^{-2}]	K_2L	-1.2577132 10^{-1}	[m^{-2}]
a_3	1.3220000 10^3	[T m^{-3}]	K_3L	3.6353697 10^2	[m^{-3}]
a_4	1.5352000 10^6	[T m^{-4}]	K_4L	1.6886595 10^6	[m^{-4}]
a_5	6.9339000 10^2	[T m^{-5}]	K_5L	3.8135083 10^3	[m^{-5}]
a_6	-1.0900000 10^1	[T m^{-6}]	K_6L	-3.5968711 10^2	[m^{-6}]
a_7	0.0	[T m^{-7}]	K_7L	0.0	[m^{-7}]
a_8	0.0	[T m^{-8}]	K_8L	0.0	[m^{-8}]
a_9	0.0	[T m^{-9}]	K_9L	0.0	[m^{-9}]
a_{10}	0.0	[T m^{-10}]	$K_{10}L$	0.0	[m^{-10}]
a_{11}	0.0	[T m^{-11}]	$K_{11}L$	0.0	[m^{-11}]
a_{12}	0.0	[T m^{-12}]	$K_{12}L$	0.0	[m^{-12}]
a_{13}	0.0	[T m^{-13}]	$K_{13}L$	0.0	[m^{-13}]

Table 5: Multipole coefficients for QM6R at $x = 0.0065$ m and $y = 0.0$ m from the center of the quadrupole from the PRIAM mapping fitted with a polynomial function using MINUIT.

vention in the MAD program), with a quadrupole component of strength -0.7121175306066 m^{-1}. Comparing with the values in Tab. 5, the dipole and quadrupole components have only slight differences of -0.03% and 0.08%, respectively. The impact on the linear optics is negligible, as shown in Fig. 11 where it is compared to standard optics of Fig. 3.

5 Field mapping for septum BS1X

The BS1X is a septum magnet that together with the septums BS2X and BS3X complete extraction from the DR to the EXT line. The lengths and angles for each septum are: BS1X (L = 0.6 m, θ=0.028035665 rad), BS2X (L = 0.8 m, θ=0.074343366 rad) and BS3X (L = 1.0 m, θ=0.235022025 rad). In the following only the field map of BS1X is computed. Fig. 12 shows the cross section top half of the BS1X septum magnet. The core is made of low carbon steel. The top part of the figure shows the different parts of the BS1X septum while the bottom

part of the figure shows the field lines calculated by POISSON [5]. The point (x=0.0 m, y=0.0 m) is at the bottom left hand corner while the right hand septum is between x=0.0937 and 0.099 m. The zone of interest for the tracking of the extracted beam is around (x=0.0855 m, y=0.0 m).
Fig. 13 shows the field lines in the computed structure (1/2 of the septum, taking into account the symmetries) calculated by PRIAM. The fit around the point $x = 0.0855$ m, within a circle of radius $r = 0.004$ m, was obtained by squared minimization and provides the normal multipole coefficients listed in Tab.6. The value of the χ^2 for this fit is 10^{-7} T^2 (for 640 sampled points).

Field Coefficient		units	**MAD Coefficient**		units
a_0	1.9961476 10^{-1}	[T]	K_0L	2.7619357 10^{-2}	
a_1	5.1208429 10^{-2}	[T m^{-1}]	K_1L	7.0853673 10^{-3}	[m^{-1}]
a_2	1.5404429 10^{1}	[T m^{-2}]	K_2L	4.2628153 10^{0}	[m^{-2}]
a_3	2.2251138 10^{3}	[T m^{-3}]	K_3L	1.8472445 10^{3}	[m^{-3}]
a_4	5.7750633 10^{4}	[T m^{-4}]	K_4L	1.9177364 10^{5}	[m^{-4}]
a_5	-6.1819396 10^{7}	[T m^{-5}]	K_5L	-1.0264243 10^{9}	[m^{-5}]
a_6	-1.9358771 10^{10}	[T m^{-6}]	K_6L	-1.9285513 10^{12}	[m^{-6}]
a_7	-3.6242908 10^{12}	[T m^{-7}]	K_7L	-2.5274029 10^{15}	[m^{-7}]
a_8	-5.0782180 10^{14}	[T m^{-8}]	K_8L	-2.8330405 10^{18}	[m^{-8}]
a_9	-4.5714786 10^{16}	[T m^{-9}]	K_9L	-2.2953062 10^{21}	[m^{-9}]
a_{10}	-6.4259328 10^{17}	[T m^{-10}]	$K_{10}L$	-3.2264143 10^{23}	[m^{-10}]
a_{11}	0.0	[T m^{-11}]	$K_{11}L$	0.0	[m^{-11}]
a_{12}	0.0	[T m^{-12}]	$K_{12}L$	0.0	[m^{-12}]
a_{13}	0.0	[T m^{-13}]	$K_{13}L$	0.0	[m^{-13}]

Table 6: Multipole coefficients for the BS1X septum at $x = 0.0855$ m and $y = 0.0$ m, obtained from the PRIAM field map by fitting a polynomial function through square minimization.

In the MAD optics description of the EXT line, BS1X is simulated as a sector bend of length (L) 0.6 m and angle 0.028035665 rad. Comparing with the value of Tab. 6, the dipole component has a difference of 1.5%. The most important normal multipole from the harmonic analysis is a small quadrupole component of 0.0070853673 m^{-1} and a small sextupole component of 4.2628153 m^{-2}. The latter is more than ten times smaller then that the obtained in the QM7R quadrupole, but still gives a tolerance level ten times bigger (0.5 $\%$ at ± 8 mm) than the tolerance level sextupole in the bends BH1X,BH2X and BH3X of the EXT line. These differences in dipole and quadrupole components have only a small impact on the linear optics. This is shown in Fig. 14, where comparison is made to the standard optics of Fig. 3 and where the only significant effect is on the horizontal beta function (β_x), whose maximum difference is about $\pm 12\%$.
It should however be mentioned that the values obtained for the multipoles in this procedure are very sensitive to the details of the shim introduced at the end of the conductor to extend the flat region of the main bend field (see Fig. 12). Moreover, it was difficult to get stable fit results

using MINUIT in this region, as large dependences on various conditions were observed, e.g. on the number of points, the boundary of the region considered or the degree of the polynom fitted. As it was found that square minimization gave stabler results, this was used for BS1X. The results were also compared with those from another computation technique for the field maps, which is available in PRIAM based on using linear Lagrange finite elements [4]. This approach is close to the approximations used in the POISSON program. The fit around the point $x = 0.0855$ m and $y = 0.0$ m, within a circle of radius $r = 0.004$ m, by squared minimization of this alternative field map gives the normal multipole coefficients listed in Tab.7. The value of the χ^2 for this fit is 1.1×10^{-7} T^2 (for 640 sampled points). The dipole component obtained is rather similar to the one in Table 6, while the quadrupolar and sextupolar components are slightly smaller, which means that they would have an even smaller impact.

Field Coefficient		units	**MAD Coefficient**		units
a_0	1.9958973 10^{-1}	[T]	K_0L	2.7615894 10^{-2}	
a_1	2.8153166 10^{-2}	[T m^{-1}]	K_1L	3.8953650 10^{-3}	[m^{-1}]
a_2	8.4796963 10^{0}	[T m^{-2}]	K_2L	2.3465575 10^{0}	[m^{-2}]
a_3	9.0493494 10^{2}	[T m^{-3}]	K_3L	7.5125871 10^{2}	[m^{-3}]
a_4	-1.0862597 10^{5}	[T m^{-4}]	K_4L	-3.6071635 10^{5}	[m^{-4}]
a_5	-7.2537976 10^{7}	[T m^{-5}]	K_5L	-1.2043913 10^{9}	[m^{-5}]
a_6	-1.8931642 10^{10}	[T m^{-6}]	K_6L	-1.8860001 10^{12}	[m^{-6}]
a_7	-3.3105246 10^{12}	[T m^{-7}]	K_7L	-2.3085977 10^{15}	[m^{-7}]
a_8	-4.3748047 10^{14}	[T m^{-8}]	K_8L	-2.4406197 10^{18}	[m^{-8}]
a_9	-4.0128670 10^{16}	[T m^{-9}]	K_9L	-2.0148314 10^{21}	[m^{-9}]
a_{10}	-8.5399590 10^{17}	[T m^{-10}]	$K_{10}L$	-4.2878515 10^{23}	[m^{-10}]
a_{11}	0.0	[T m^{-11}]	$K_{11}L$	0.0	[m^{-11}]
a_{12}	0.0	[T m^{-12}]	$K_{12}L$	0.0	[m^{-12}]
a_{13}	0.0	[T m^{-13}]	$K_{13}L$	0.0	[m^{-13}]

Table 7: Multipole coefficients for BS1X at $x = 0.0855$ m and $y = 0.0$ m from the center of the septum magnet from the PRIAM linear Lagrange method of mapping, fitted with a polynomial function by square minimization.

6 Non-linear fields in BS2X and BS3X septum magnets

The septum magnets BS2X and BS3X are further away from the damping ring than BS1X. This makes the geometry less constrained and their placement easier. From the corresponding engineering drawings, the nominal position of the extracted beam is 15.3 and 16 mm from the septum conductor for BS2X and BS3X respectively, in comparison to 8.2 mm for BS1X (see Table 1). This means that the beam passes farther away from the delicate region near the

edge of these magnet where shims are included to help flatten the field. The non-linearity was checked to be small enough to be neglected in this region.

7 Conclusions

We have calculated the field map and multipolar components for the shared magnets of the ATF extraction line using the code PRIAM. The calculations are compatible with the POISSON calculations from [5]. Since the PRIAM field map has a finer mesh, the corresponding multipolar components should be more accurate for use in future linear and non-linear optics calculations or in tracking simulations of the ATF EXT line.
Furthermore, the impact on the linear optics of the modified dipole and quadrupole components obtained from these field maps has been evaluated. Fig. 15 shows the impact taking into account the effect of all three elements analyzed: QM7R, QM6R and BS1X. Contributions from QM6 and BS1X magnets are negligible compared to the large deviation of the quadrupole strength of QM7, and hence, the results are rather similar to Fig. 9.

Acknowledgments

We would like to acknowledge the ATF group at KEK for supporting this effort and Cherrill Spencer for providing details of the POISSON calculation made at SLAC. We acknowledge as well the support of the European Community-Research Infrastructure Activity under the FP6 “Structuring the European Research Area” programme (CARE, contract number RII3-CT-2003-506395).

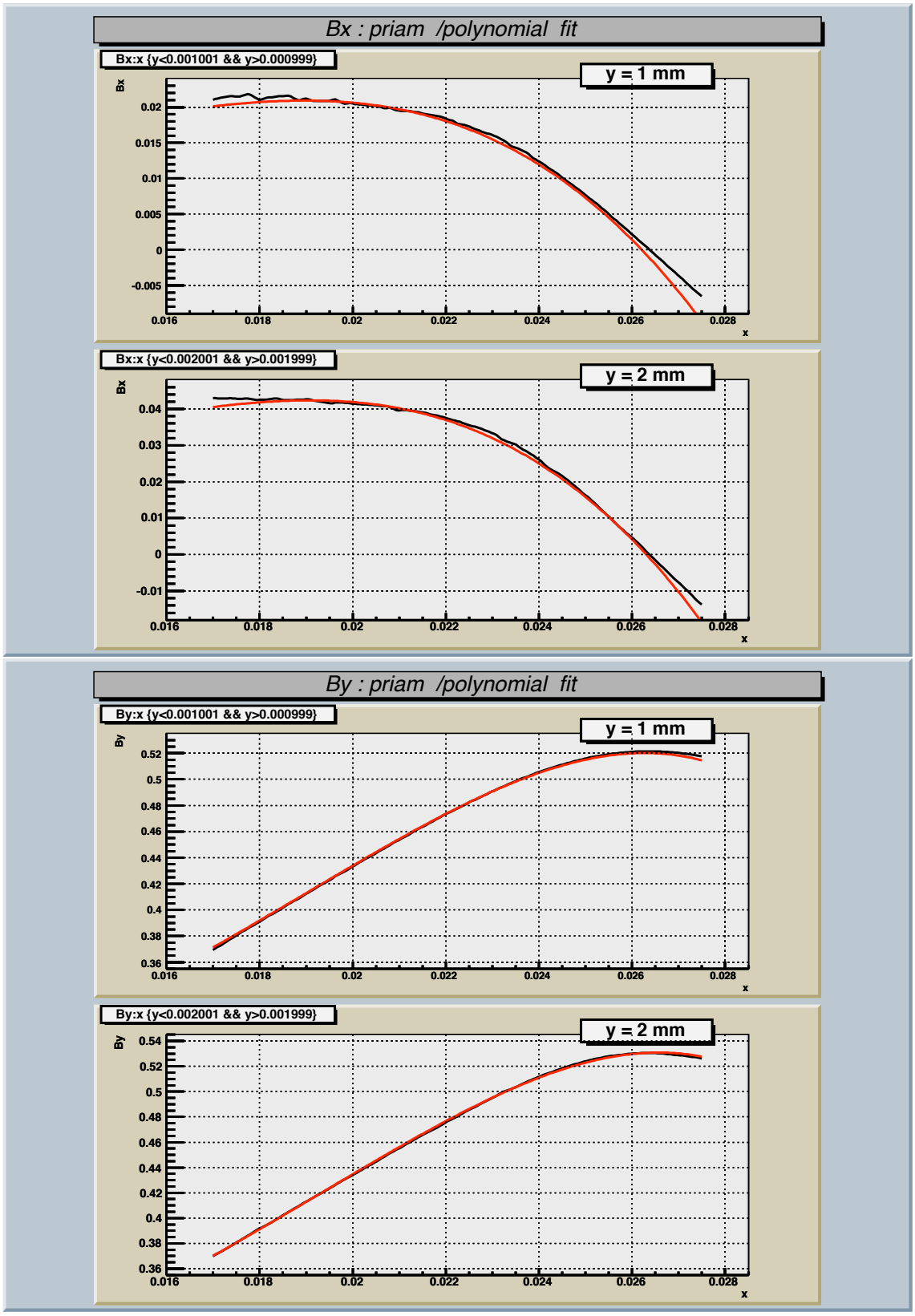

Figure 6: (a) QM7R Bx at y= 1, 2 mm; (b) QM7R By at y= 1, 2 mm.

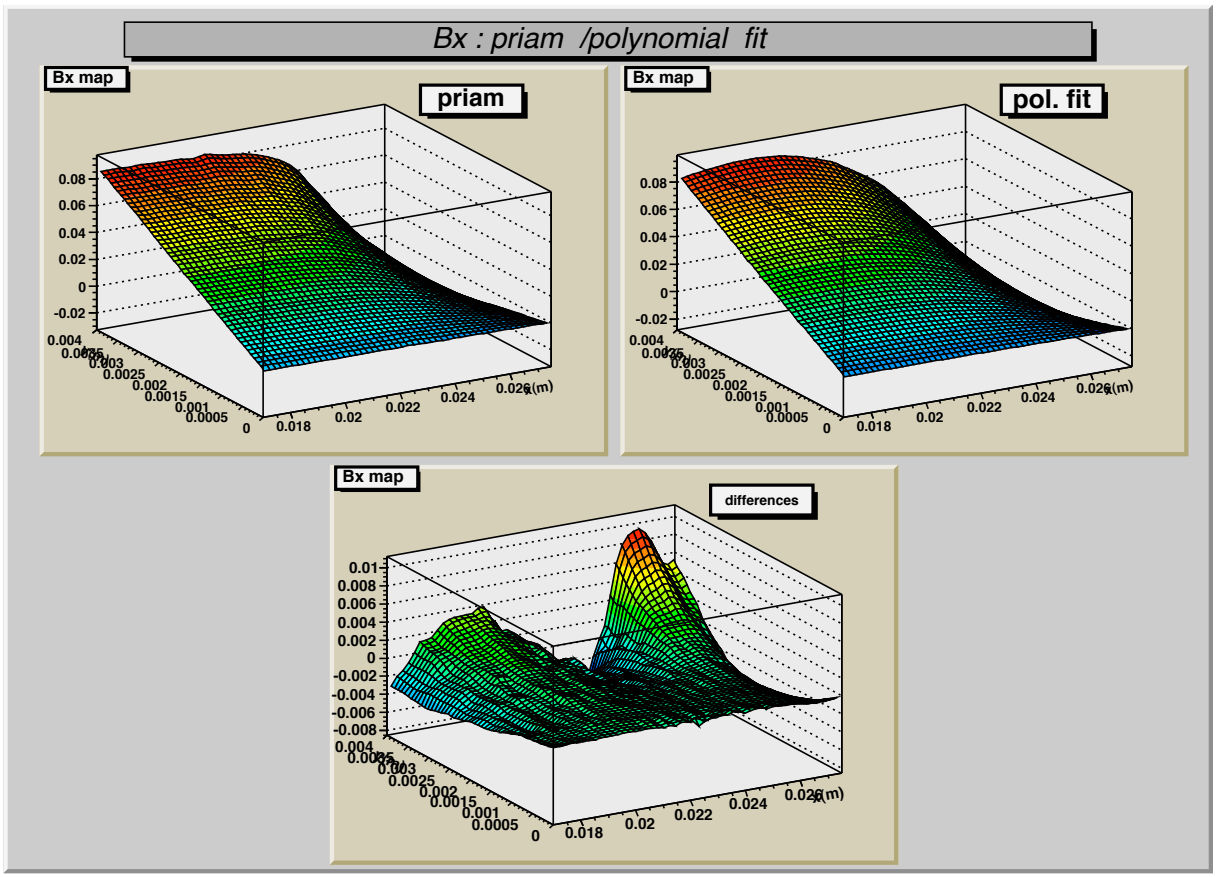

Figure 7: QM7R B_x: comparison of PRIAM and fitted values.

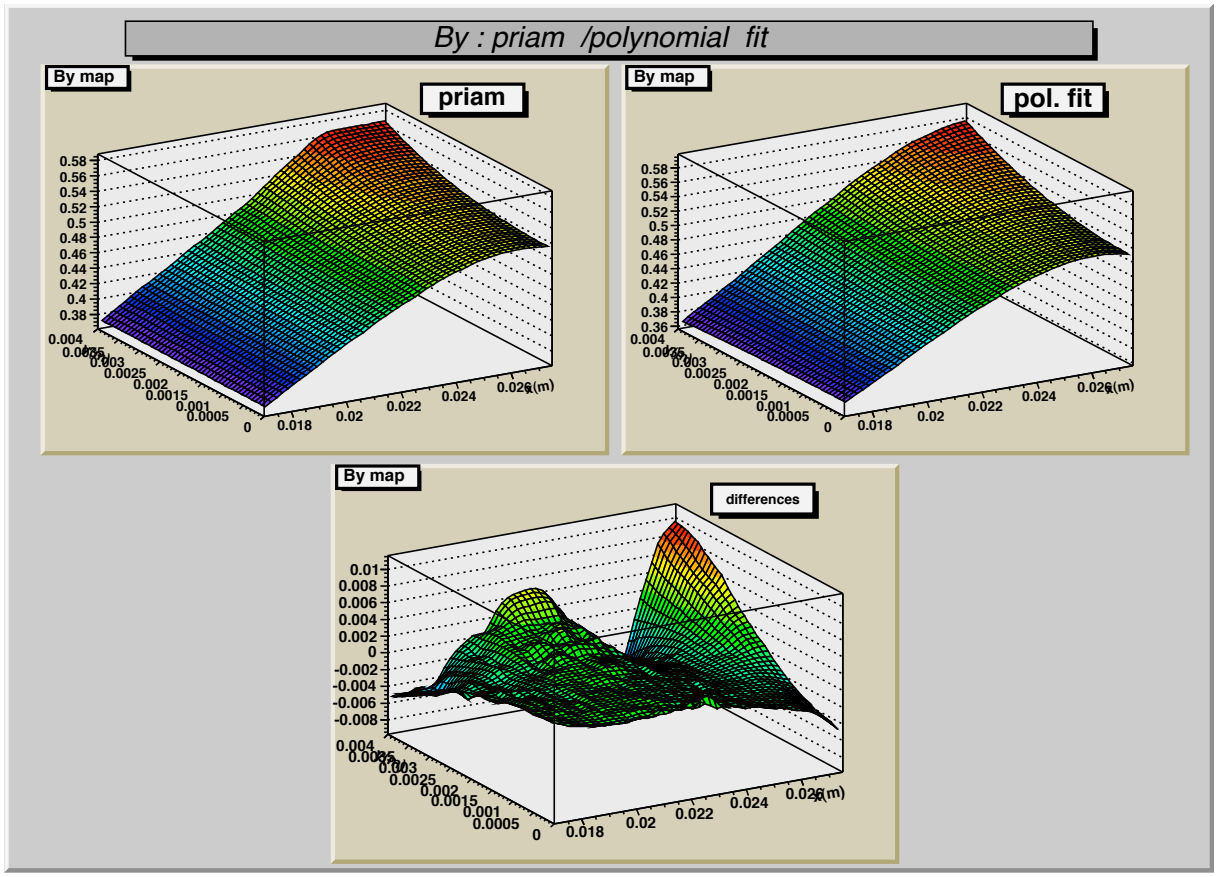

Figure 8: QM7R B_y: comparison of PRIAM and fitted values.

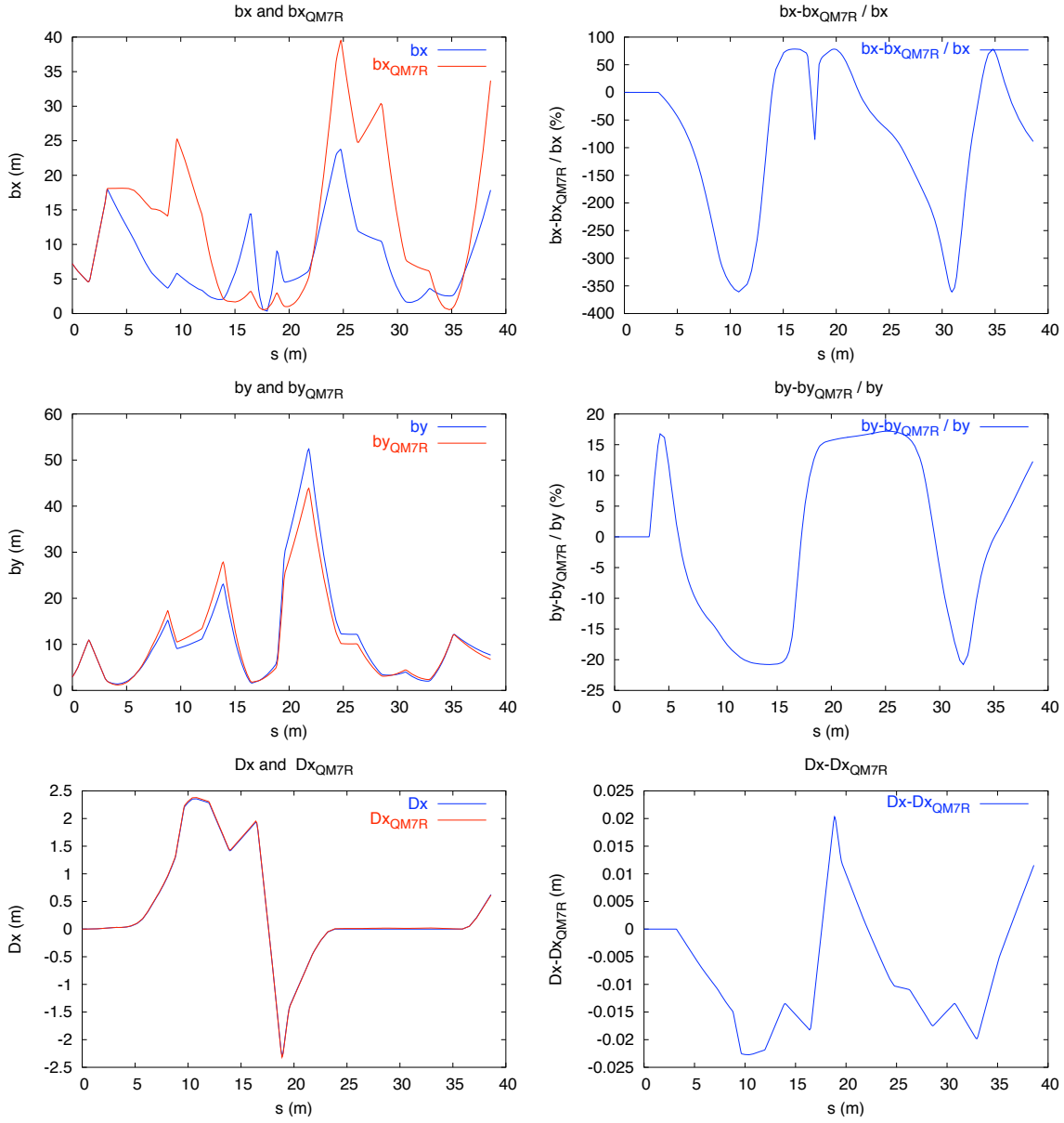

Figure 9: Relative differences between the standard optics functions in the ATF EXT line and those computed with the values of the dipole and quadrupole components of QM7R calculated by PRIAM for the extracted beam.

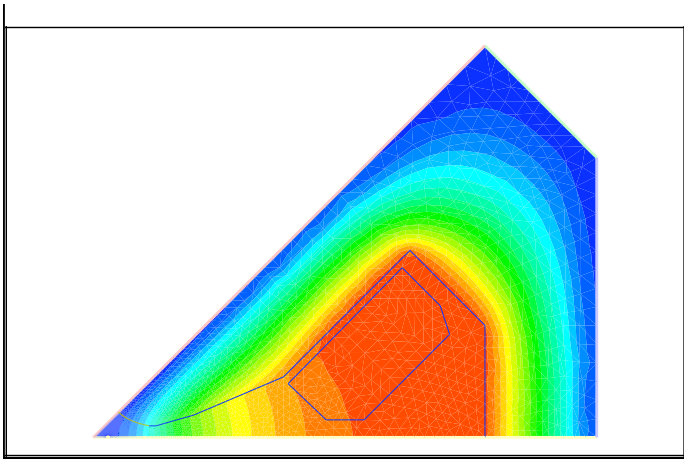

Figure 10: QM6R B field lines

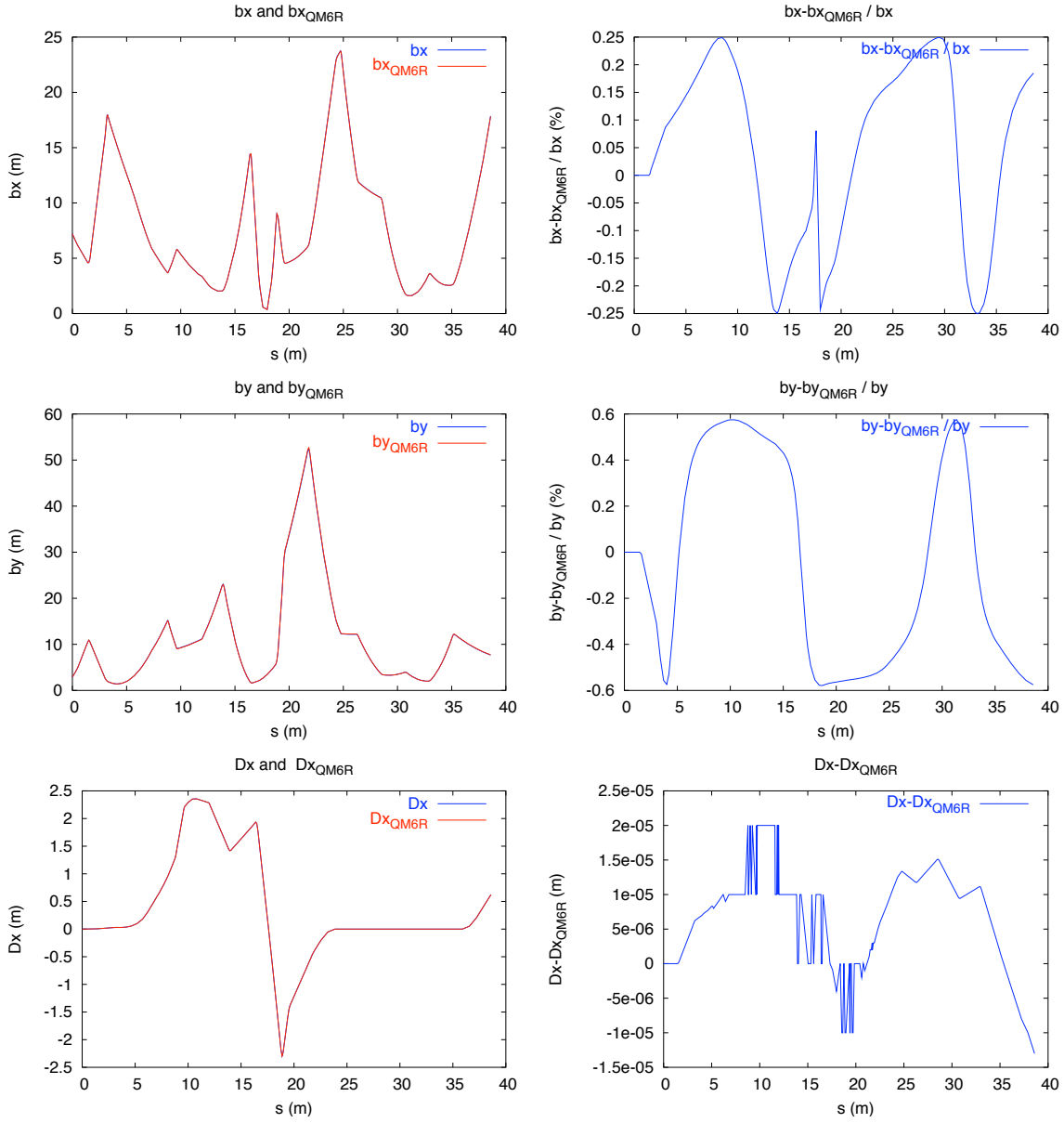

Figure 11: Relative differences between the standard optics functions in the ATF EXT line and those computed with the values of the quadrupole and dipole components calculated for QM6R by PRIAM at the location of the extracted beam.

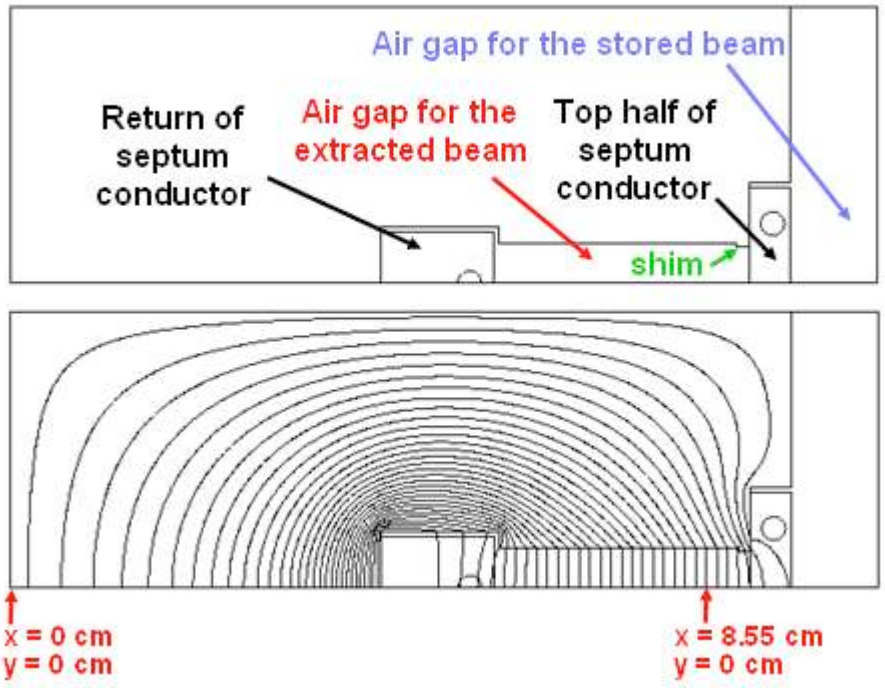

Figure 12: Top:Cross section trough top half of BS1X septum magnet. Bottom:Field lines of BS1X calculated with POISSON.

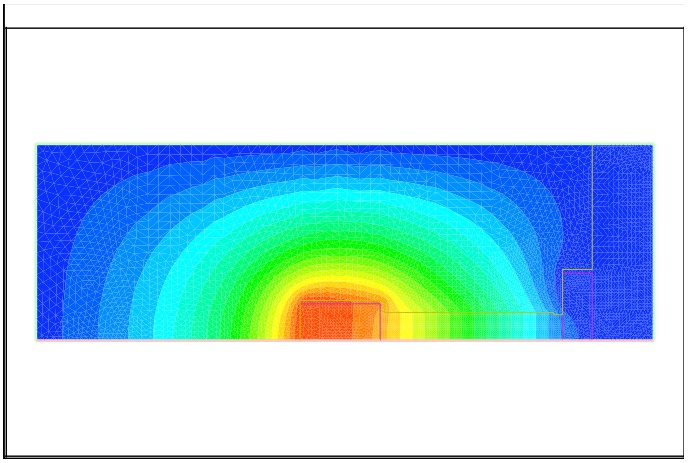

Figure 13: BS1X B field lines computed with PRIAM

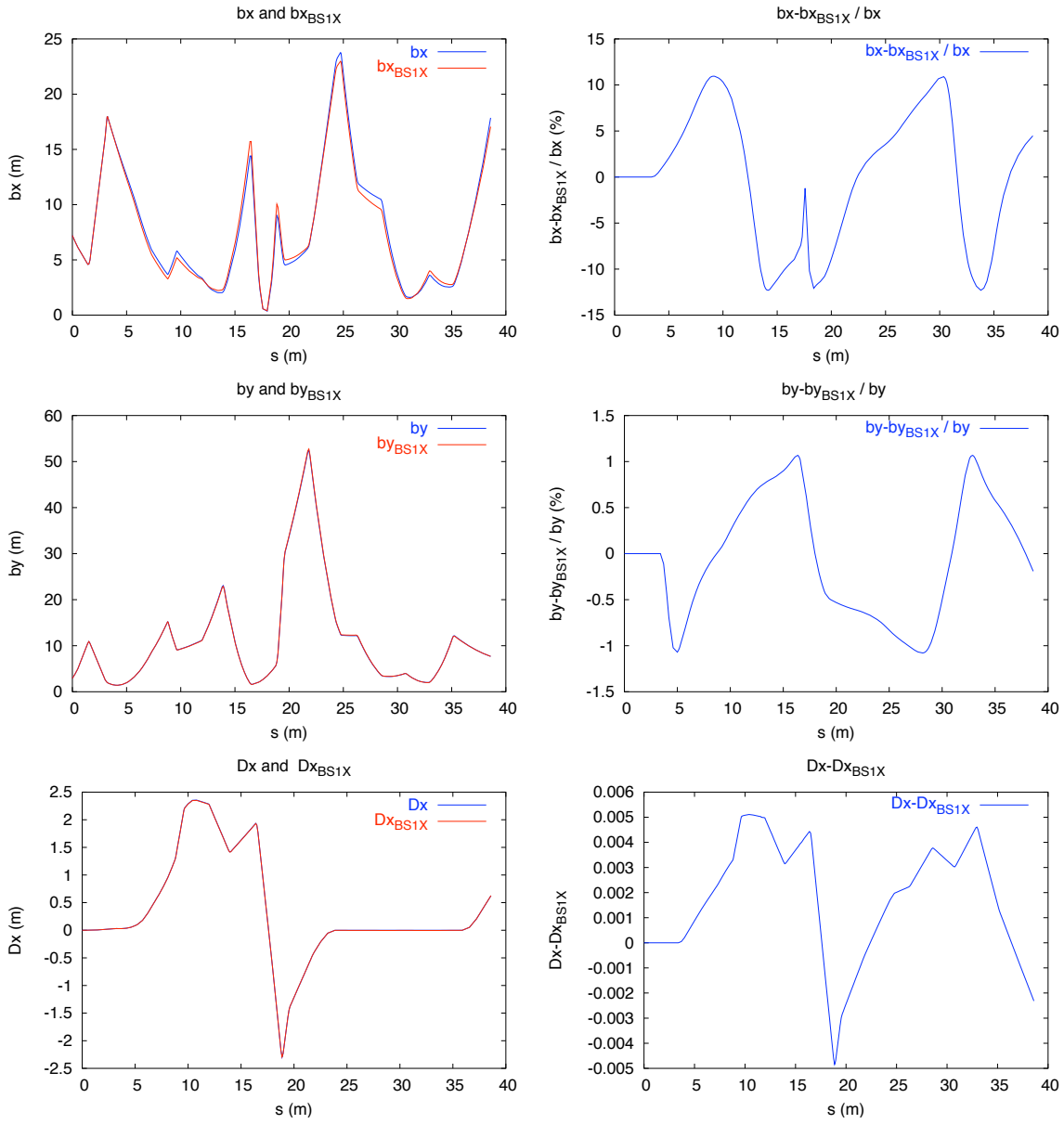

Figure 14: Relative differences between the standard optics functions in the ATF EXT line and those computed with the values of the dipole and quadrupole components calculated for BS1X by PRIAM at the location of the extracted beam.

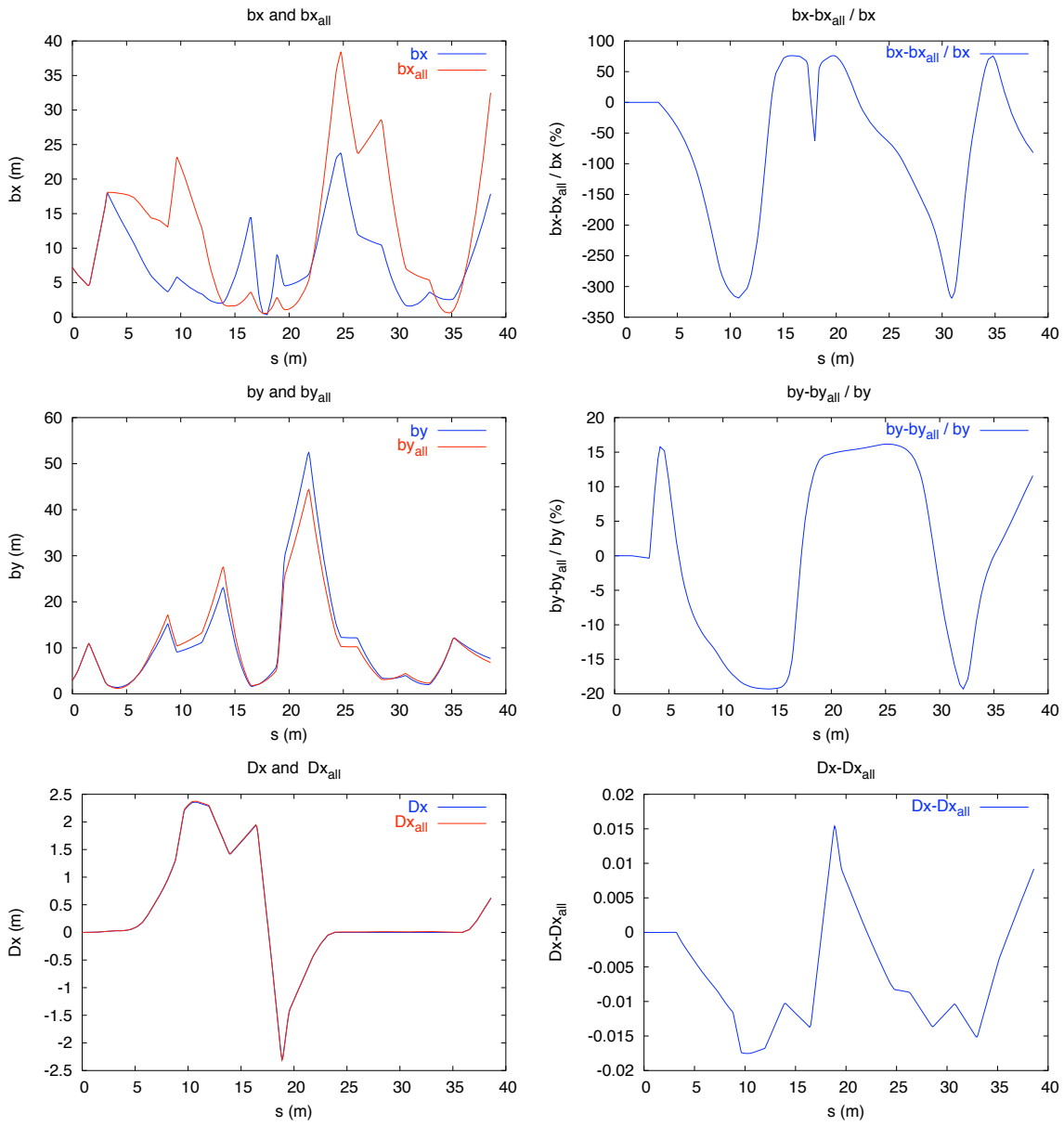

Figure 15: Relative differences between the standard optics of the ATF EXT line and with the value of: QM7R, QM6R and BS1X calculated by PRIAM.

References

[1] "ATF Report". Study report JFY 1996-1999, http://atfweb.kek.jp./atf/Reports/ATF99new.pdf.

[2] "ATF2 Proposal, Vol. 1 and 2", ATF Collaboration, August 11 2005 and February 13 2006, http://lcdev.kek.jp/ATF/proposal.

[3] J. Nelson, M. Ross, M. Woodley, "ATF Studies: Extraction line dispersion, beam stability and bunch length sensitivity, etc", June 2000, ATF-00-06 Internal Report.

[4] G. Lemeur and F. Touze,"PRIAM / ANTIGONE a 2D 3D package for Accelerator Design", EPAC 94.

[5] F. Zhou, J. Amann, S. Selestky, C. Spencer and M. Woodley, "Simulation studies on the Vertical Emittance Growth in the Existing ATF Extraction BeamLine", SLAC-PUB-12892 December 2007.

[6] H. Grote and F.C. Iselin, "The MAD program (Methodical Accelerator Design) version 8.16, User's reference manual", CERN/SL/90-13(AP), (rev. 4), (March 27, 1995).

[7] "CERN MINUIT Package", http://www.cern.ch/minuit.

8 Appendix 1: Finite element computation of the magnetic field

8.1 Magnetostatic equations

Let Ω be an open domain in the R2 space of real numbers with smooth boundary Γ. Maxwell's equations and potential vector equation reduce in the magnetostatic case to:

$$\begin{cases} rot\vec{H} = j \\ div\vec{B} = 0 \\ \vec{B} = \vec{rot}A \quad where \quad \vec{B} = \mu\vec{H} \end{cases}$$

$\vec{H}$ is the magnetic field, $\vec{B}$ the magnetic flux density, j is the applied source current and μ is the permeability. The condition $\vec{H} \wedge \vec{n} = 0$, where $\vec{n}$ is the normal boundary vector, is imposed over all conducting boundaries.

8.2 Finite element model

The finite element code PRIAM [4] uses so-called edge elements, which are very well suited to the mathematical structure of Maxwell's equations. A brief description of the principle of the formulation follows.
Galerkin's approximation is applied to the equations defined above in two dimensions, in order to find the solution of :

$$\begin{cases} \iint \vec{B} \cdot \vec{p}\, dxdy = \iint \vec{rot}A \cdot \vec{p}\, dxdy \\ \iint rot\vec{H}\, q\, dxdy = \iint j\, q\, dxdy \end{cases}$$

where $\vec{p}$ and $\vec{q}$ are weighting functions.
Applying Green's theorem (integration by parts) leads to :

$$\begin{cases} \iint \mu\vec{H} \cdot \vec{p}\, dxdy = \iint A\, rot\vec{p}\, dxdy + \int A\, (\vec{p} \wedge \vec{n})\, ds \\ \iint rot\vec{H}\, q\, dxdy = \iint j\, q\, dxdy \end{cases}$$

According to the general scheme of Galerkin, the finite dimensional space $\vec{H}$ is introduced which ensures the existence of the integrals written above. So, we look for the field in space $\vec{H}$, assumed to be a linear combination of basis functions. The coefficients of this combination, the unknowns of the problem, are the circulations of $\vec{H}$ along the edges of the (triangular) elements of the mesh. Finally, thanks to this approximation, we exhibit a linear system and determine $\vec{H}$.